

RESEARCH

Open Access



LGALS3BP antibody-drug conjugate enhances tumor-infiltrating lymphocytes and synergizes with immunotherapy to restrain neuroblastoma growth

Ilaria Cela^{1,2}, Emily Capone^{2,3}, Asia Pece², Giulio Lovato^{1,2}, Pasquale Simeone^{2,4}, Martina Colasante⁵, Alessia Lamolinara^{2,6}, Anna Piro⁷, Manuela Iezzi^{2,6}, Paola Lanuti^{2,4}, Vincenzo De Laurenzi^{1,2}, Rodolfo Ippoliti⁵, Stefano Iacobelli⁸ and Gianluca Sala^{1,2*} 

Abstract

Background LGALS3BP, also referred as Gal-3BP, Mac2-BP, or 90 K, is a heavily glycosylated, secreted protein prominently localized at the surface of cancer-derived extracellular vesicles (EVs). Its levels are significantly elevated in various types of cancer, including neuroblastoma, and are generally associated with advanced disease and tumor progression. Our previous research has shown that LGALS3BP is an effective target for ravtansine (DM4)-based Antibody-Drug Conjugate (ADC) therapy in multiple preclinical models.

Methods We assessed total and extracellular vesicles (EVs)-associated LGALS3BP through ELISA assay in serum of a pseudometastatic neuroblastoma model to evaluate the correlation of LGALS3BP levels with tumor dissemination. We employed a syngeneic neuroblastoma mouse model using murine neuroblastoma NXS2 cells overexpressing human LGALS3BP in order to evaluate immunogenic cell death (ICD) induced by anti-LGALS3BP ADC therapy and investigated the nature of the tumor immune infiltrate by cytofluorimetry. Furthermore, we designed a six-arm in vivo experiment to evaluate the efficacy of ADC in combination with an immune check-point inhibitor (ICI) anti-PD-1. Finally, a rechallenge assay was conducted on cured mice to assess the presence of immunological memory.

Results Here, we report that circulating and EVs-associated LGALS3BP levels significantly correlate with neuroblastoma progression and dissemination. Moreover, we show that in the syngeneic NXS2 neuroblastoma model, DM4 treatment induces cell surface expression of ICD markers calreticulin, HSP70, and HSP90, and an increased PD-L1 expression in vitro, followed by enhanced tumor-infiltrating lymphocytes in vivo. Notably, the combination therapy of anti-LGALS3BP-targeting ADC with anti-PD-1 results in a higher inhibition of tumor growth and prolonged survival compared with either agent given alone. Rechallenge assay reveals that mice previously treated and cured with the ADC retain immune memory, suggesting the therapy's ability to induce a durable and protective antitumor immune response.

*Correspondence:

Gianluca Sala
g.sala@unich.it

Full list of author information is available at the end of the article



© The Author(s) 2025. **Open Access** This article is licensed under a Creative Commons Attribution-NonCommercial-NoDerivatives 4.0 International License, which permits any non-commercial use, sharing, distribution and reproduction in any medium or format, as long as you give appropriate credit to the original author(s) and the source, provide a link to the Creative Commons licence, and indicate if you modified the licensed material. You do not have permission under this licence to share adapted material derived from this article or parts of it. The images or other third party material in this article are included in the article's Creative Commons licence, unless indicated otherwise in a credit line to the material. If material is not included in the article's Creative Commons licence and your intended use is not permitted by statutory regulation or exceeds the permitted use, you will need to obtain permission directly from the copyright holder. To view a copy of this licence, visit <http://creativecommons.org/licenses/by-nc-nd/4.0/>.

Conclusions Our findings establish that circulating LGALS3BP is a potential biomarker for liquid biopsy and uncover this protein as a suitable target for therapeutic strategies combining 1959-sss/DM4 ADC with an anti-PD-1 ICI for the treatment of LGALS3BP expressing neuroblastoma.

Introduction

Neuroblastoma (NB) is the most common and aggressive extracranial solid tumor of pediatric age [1]. Almost half of NB patients show high metastatic potential and a 5-year survival rate approximately of 50% [2]. Currently, diagnosis of NB relies on biopsy and clinical symptoms, making early intervention difficult besides issues related to histological invasiveness [3] and disease's heterogeneity [4]. Therefore, identification of reliable and early detectable biomarkers is of primary importance. In this context, detection and quantification of circulating EVs released by cancer cells may serve as an innovative and promising tool for liquid biopsy [5, 6], facilitating tracking of neuroblastoma progression and therapeutic response [7].

To date, high risk NB patients undergo a multimodal therapeutic regimen consisting of a combination of surgery, chemo- and radiation therapy, and, as recently enclosed, immunotherapy [8], which has significantly improved patient outcomes through the introduction of dinutuximab, a monoclonal antibody targeting the surface antigen GD2 [8]. However, long-term side-effects and high rates of toxicity indicate the need of finding new therapeutic approaches. As far as immune check-point inhibitors (ICIs), the inconsistent clinical responses to these agents [9] seems to support the notion of neuroblastoma as an “immunologically cold” tumor [10], with general absence of tumor-reactive infiltrating T cells in most cases [11, 12].

Combination immunotherapies based on the association of Antibody Drug-Conjugates (ADCs) with ICIs has gained great interest in recent years, with the demonstration of a synergistic anti-tumor effect due to the stimulating of the host's immune responses and turning on the immunological cold tumor microenvironment (TME) of neuroblastoma into a “hot” and highly T-cells infiltrated one [13, 14]. This therapeutic combination would take advantage by the use of ADCs' cytotoxic payloads able to induce immunogenic cell death (ICD), a type of death of cells that releases typical damage-associated patterns (DAMPs) acting as signals for antigen-presenting cells (APCs), which in turn prime adaptive immune responses, especially involving T cells [15].

LGALS3BP (also known as Gal-3BP, Mac2-BP or 90 K) is a heavily glycosylated protein found to be overexpressed in several types of human cancer and involved in various cellular processes, including immune response modulation, cell adhesion, and signaling [16]. As a matter of fact, LGALS3BP has emerged as a

crucial factor in regulating cancer-stroma interactions and is one of the most abundant surface components of cancer-derived EVs. Importantly, recent findings have reported the contribution of LGALS3BP in the cross-talk between neuroblastoma and tumor stroma cells and the LGALS3BP-dependent secretion of pro-tumorigenic cytokines (i.e., IL-6) from mesenchymal stem cells (MSCs) after internalization of neuroblastoma-derived EVs [17–19]. Specifically, LGALS3BP levels are significantly elevated in various cancers, including neuroblastoma, and can be detected in body fluids such as blood or urine, making this molecule a promising candidate for non-invasive diagnostic approaches. Here, we present evidence of the potential role of circulating LGALS3BP as a neuroblastoma biomarker for liquid biopsy. Additionally, we provide evidence for a role of the protein as a potential therapeutic target for ADC therapy in combination with immunotherapy.

Materials and methods

Cell lines and reagents

Human neuroblastoma SKNAS cells were purchased from American Type Culture Collection (ATCC; Rockville, MD, USA). The NXS2 murine neuroblastoma cell line was kindly provided by Holger N. Lode (University Medicine Greifswald, Germany) [20]. SKNAS, parental NXS2 cells, and stable-transduced NXS2 CTRL and hLGALS3BP cells were all cultured in Dulbecco's modified Eagle's medium (DMEM, Gibco; Waltham, MA, USA) supplemented with 10% heat-inactivated fetal bovine serum (FBS) (Gibco), 100U/mL penicillin and 100 µg/mL streptomycin (Sigma-Aldrich Corporation, St. Louis, MO, USA). All cells were maintained at 37 °C in a humidified air with 5% CO₂. All cell lines were tested for mycoplasma contamination through polymerase chain reaction (PCR).

SH-DM4 was purchased from MedChemExpress (HY-12454; New Jersey, USA). Oxaliplatin was purchased from Sigma-Aldrich (#O9512). Anti-mouse PD-1 monoclonal antibody (InVivoMab, CD279; clone RMP1-14, #BE0146) was purchased from BioXCell (NH, USA).

Stable lentiviral transduction

NXS2 CTRL and NXS2 hLGALS3BP cell lines were obtained by stable lentiviral transduction starting from NXS2 parental cell lines. Lentivirus particles were produced by transient co-transfection of packaging cell line HEK 293T with a three-plasmid expression system using Lipofectamine 2000 (Invitrogen, Thermo-Fisher,

Waltham, MA, USA). Lentiviral plasmid pLenti-CMV-PURO-hLGALS3BP for stable overexpression of human LGALS3BP cDNA was obtained as follows: custom cloning was performed by Genscript (USA) by inserting human LGALS3BP cDNA in XbaI/SalI sites of the backbone pLenti-CMV-GFP-PURO (685-5) plasmid and excluding GFP sequence, a gift from Eric Campeau & Paul Kaufman (Addgene plasmid #17488, <http://n2t.net/addgene:17448>; RRID: Addgene_17448) [21]. Control plasmid (empty vector) pLenti-CMV-PURO was purchased from Origene (S100092; MD, USA). Briefly, HEK 293T cells were incubated for 6 h with transfection reagents. Lentiviral particles were collected after 48 and 72 h and filtered through 0.45 µm pore sterile filters (Corning, NY, USA). The day before the first cycle of transduction, 2×10^5 NXS2 cells were plated. After 24 h cells were incubated for 6 h with media containing viral particles together with 4 µg/mL of polybrene to increase transduction efficiency. After the first cycle of transduction, cells were washed and cultured with fresh medium overnight before a second cycle of transduction the day after. Cells were then let grow under standard growth conditions for 72 h before being put under selection with 1 µg/mL of puromycin (Sigma-Aldrich). Selection was maintained throughout all experiments performed. LGALS3BP levels were assessed through quantitative real-time PCR (qRT-PCR), western blotting and ELISA analysis.

Western blotting

Murine neuroblastoma cells (5×10^5) were seeded in complete medium and after 48 h they were lysed in RIPA buffer (50mM Tris/HCl pH 7.6, 150mM NaCl, 1% NP-40, 0.5% Na-Deoxycholate, 0.1% SDS, 1mM EDTA pH 8) containing protease inhibitor cocktail (Sigma-Aldrich), phosphatase inhibitor cocktail (Roche, Thermo-Fisher), and Na_3VO_4 (Sigma-Aldrich). Lysates were clarified by centrifugation at 13,000 rpm for 30 min at 4 °C. Equal amounts of protein lysates (20 µg per sample), previously heated at 95 °C for 5 min, were subjected to SDS-PAGE electrophoresis and then electrotransferred to nitrocellulose membranes for Western blot analysis. Membranes were blocked for 1 h at RT with 5% non-fat dry milk in PBS with 0.1% Tween20. Membranes were then incubated overnight at 4 °C with the following primary antibodies: anti-human LGALS3BP (goat polyclonal; 1:1000, #AF2226; R&D Systems, MN, USA); anti-β-actin (mouse monoclonal; 1:40000, #A5441; Sigma-Aldrich). After three washes in PBS-0.1% Tween20, the membranes were hybridized with horseradish peroxidase (HRP)-conjugated secondary antibodies (goat or mouse; Biorad, CA, USA). Detection of signal bands was performed with Clarity Western ECL substrate (#1705061; Biorad). Images of membranes were acquired with a UvitecFire

reader (Cambridge, UK) and analysed with Alliance Uvitec software (Cambridge, UK).

Quantitative reverse transcription-PCR (qRT-PCR)

A total of 5×10^5 murine neuroblastoma cells were cultured in complete medium for 48 h, then total RNA was isolated from collected cells by RNeasy kit (#74136; Qia-gen, Germany). One microgram of total RNA was reverse transcribed to cDNA by using High-capacity cDNA reverse transcription kit (#4368814; Applied Biosystems, MA, USA) according to the manufacturer's instructions. Real-time qPCR was performed with a CFX96 Touch Real-Time PCR Detection system (Biorad) using SsoAdvanced Universal SYBR Green supermix (#1725271; Biorad), according to manufacturer's instructions. The primers used at a final concentration of 350nM were: hLGALS3BP FOR 5'-GAA CCC AAG GCG TGA ACG AT-3'; hLGALS3BP REV 5'- GTC CCA CAG GTT GTC ACA CA-3'; h-β-actin FOR 5'- CAG CTC ACC ATG GAT GAT GAT ATC-3'; h-β-actin REV 5'-AAG CCG GCC TTG CAC AT-3'; mLGALS3BP FOR 5'-TCT CTT GCT CCC AGG GTT GG-3'; mLGALS3BP REV 5'-CCG TTA ACC AAG CGC ATG TC-3'; m-β-actin FOR 5'-CTA AGG CCA ACC GTG AAA AG-3'; m-β-actin REV 5'-ACC AGA GGC ATA CAG GGA CA-3'. Each sample analysis was performed in triplicate. As a negative control, a no template control was performed. The following PCR program was used: 95 °C for 30s, 40 cycles of denaturation at 95 °C for 15s and annealing/extension at 57 °C for 30s. In order to verify the specificity of the amplification, a melting curve analysis was performed immediately after the amplification protocol. qRT-PCR results were calculated using the $\Delta\Delta\text{Ct}$ method and normalized using human or mouse β-actin as reference gene.

Immunofluorescence and confocal imaging

For confocal live cell staining, 2×10^5 NXS2 CTRL or NXS2 hLGALS3BP were plated on glass coverslips in 12-well plates and cultured under standard growth conditions. After 24 h, cells were incubated for 90 min at 37 °C with 10 µg/mL of anti-LGALS3BP antibody 1959 in PBS $\text{Ca}^{2+}/\text{Mg}^{2+}$ with 3% BSA. Cells were then fixed with 4% paraformaldehyde for 10 min at RT and stained with anti-human AlexaFluor-488 conjugated secondary antibody (1:200, #A11013; Invitrogen) and Hoechst3342 (1:500; Sigma-Aldrich) for 30 min at RT in the dark. Confocal images were acquired using a Zeiss LSM800 inverted confocal microscope system (Carl Zeiss, Germany).

Enzyme-linked immunosorbent assay (ELISA)

A total of 5×10^5 murine neuroblastoma cells were cultured in complete medium for 48 h before supernatants were collected. Secreted human LGALS3BP levels were

evaluated by sandwich ELISA that was performed as follows: Maxisorp 96-well plates (Nunc, Thermo-Fisher) were coated with murine anti-LGALS3BP antibody SP2 [22] [2 µg/mL] overnight at 4 °C. After blocking with 1% bovine serum albumin (BSA) in PBS for 1 h at RT, 100 µl of cell culture media were added and incubated for 1 h at RT. After three washes with PBS-0.05% Tween20, humanized anti-LGALS3BP antibody 1959 [1 µg/mL] was incubated for 1 h at RT. For the detection, after three washes with PBS-0.05% Tween20, anti-human IgG-HRP (#A01070; Sigma-Aldrich) was added (1:5000) and incubated for 1 h at RT. After three washes, stabilized chromogen was added for at least 10 min in the dark before stopping the reaction with the addition of 1 N H₂SO₄. The resulting color was finally read at 450 nm with an ELISA plate reader (Tecan, Switzerland). Secreted mouse LGALS3BP levels were assessed by using mouse Galectin-3-Binding protein (LGALS3BP) ELISA kit according to manufacturer's instructions (#MBS9717790; MyBioSource, CA, USA).

For the evaluation of serum and EVs-associated human LGALS3BP levels in human neuroblastoma pseudo-metastatic experiments, human LGALS3BP ELISA Kit was performed according to manufacturer's instructions (#KE00155; Proteintech, USA). In particular, EVs samples were isolated from mouse serum by using ExoQuick Exosome Precipitation Solution (#EXOQ5A-1; System Biosciences, CA, USA) according to manufacturer's instructions. Once isolated, EVs were quantified with Bradford assay (Biorad) and read in a 96-well plate reader (Tecan).

Extracellular vesicles (EVs) purification and analysis from cell culture media

Once reached the 80% confluence, NXS2 CTRL or NXS2 hLGALS3BP cells were grown for 48 h in serum-free medium. Around 100 mL of cell culture supernatant was collected, and differential ultracentrifugation was performed for EVs isolation. Briefly, supernatants were centrifuged at 2000 g and 10,000 g for 20 and 30 min, respectively, at 4 °C to remove dead cells and cellular debris. Then, to collect exosomes, supernatants were ultracentrifuged at 100,000 g for 70 min at 4 °C and then washed with PBS and re-collected by centrifugation at 100,000 g for 70 min at 4 °C. Protein content was quantified by Bradford assay (Biorad) prior to western blotting analysis, besides whole-cell lysates previously lysed in RIPA buffer as previously described. Blots were then probed with anti-human LGALS3BP (goat polyclonal; 1:1000, #AF2226; R&D Systems), anti-β-actin (mouse monoclonal; 1:40000, #A5441; Sigma-Aldrich), anti-Alix (mouse monoclonal; 1:500, #MA1-83977; Invitrogen), anti-Tsg101 (mouse monoclonal; 1:1000, #MA1-23296; Invitrogen).

Nanoparticle tracking analysis (NTA)

Size and concentration of EVs were characterized by nanoparticle tracking analysis (NTA) on a ZetaView system (Particle Metrix, Meerbusch, Germany) equipped with a blue laser (488 nm, 40 mW) and a long-pass emission filter. The autofocus was calibrated to ensure optimal particle visualization. Consistent and optimized post-acquisition settings were applied throughout the analyses. Each sample was analyzed by capturing videos across 11 fields, with the resulting measurements compiled into reports detailing all relevant parameters, such as mean and median EV sizes.

Cytotoxicity assay

Murine neuroblastoma cells were cultivated into 24-well plates at a density of 8×10^3 cells per well under standard growth conditions. After 24 h, cells were treated for 72 h with increasing doses of SH-DM4 (from 0.00064nM to 250nM) or naked 1959-sss antibody (from 0.0064nM to 100nM). At the end of treatments, cells were incubated with 3-(4,5-dimethylthiazol-2-yl)-2,5-diphenyltetrazolium bromide (MTT) solution (medium serum-free with 0.5 mg/mL of MTT) for 2 h. After the removal of the MTT solution, dimethylsulfoxide (DMSO) was added to each well and then the absorption value at 570 nm was measured using a multi-plate reader (Tecan). All experiments were performed in triplicate at least in two independent experiments. IC₅₀ (Inhibition of cellular proliferation by 50%) values were calculated by using GraphPad Prism 9.0 software (GraphPad Software, Inc., CA, USA).

FACS analysis of ICD markers and PD-L1 levels

For the evaluation of surface ICD markers, 5×10^5 NXS2 cells were plated and treated or not with SH-DM4 (DM4) 5nM or Oxaliplatin (OXA) 60µM for 72 h in complete medium. All cells were harvested after 24, 48 and 72 h from treatment and labelled for 30 min in ice with the following primary antibodies: anti-mouse calreticulin (rabbit monoclonal; 1:800, #12238, clone D3E6; Cell Signaling Technology, USA), anti-mouse HSP70 (rabbit polyclonal; 1:400; #NBP1-77455; Novus Biologicals, USA), or anti-mouse HSP90 (mouse monoclonal; 1:100, #ADI-SPA-830, clone AC88; Enzo Life Sciences, USA). After washing, cells were labelled for 30 min at 4 °C in the dark with AlexaFluor-488 conjugated secondary antibodies (anti-mouse or anti-rabbit; 1:1000, #A28175 or #A27034; Thermo-Fisher). Samples were acquired by FACSCanto II cytometer (BD Biosciences) and analysis was performed using a BD FACSDiva v.8.0.3 (BD Biosciences).

For the evaluation of PD-L1 levels, 5×10^5 NXS2 cells were plated and treated with DM4 3nM for 72 h. Cells were harvested and fixed for 15 min at RT with 4%

paraformaldehyde. After washing, cells were permeabilized for 15 min at RT with 0.1% Triton X-100 and labelled for 30 min at 4 °C with primary antibody anti-PD-L1 (rabbit polyclonal; 1:100, #PA5-20343; Invitrogen). Then cells were labelled for 30 min at 4 °C in the dark with AlexaFluor-488 conjugated anti-rabbit secondary antibody (1:300, #A27034; Thermo-Fisher). Samples were acquired by FACSCanto II cytometer (BD Biosciences) and analysis was performed using a BD FACSDiva v.8.0.3 (BD Biosciences).

In vivo mouse models and treatments

Human neuroblastoma pseudometastatic NSG mouse model

NSG mice were purchased from Jackson Laboratory and bred in the animal facility of CAST, G. d'Annunzio University of Chieti. Animal care and experimental procedures were approved by the Ethics Committee for Animal Experimentation of the Institute according to Italian law (Authorization n° 1118/2020-PR). The animal health status was monitored daily, and body weight was measured once a week during experiments. For the evaluation of LGALS3BP levels in correlation with metastatic lesions, 8-weeks male NSG were tail-vein injected with 1×10^6 SKNAS cells and blood was collected after 7, 14, 21, or 28 days after injection. Blood was collected by intracardiac puncture immediately after mice sacrifice in a tube containing a glass Pasteur pipette to induce blood clotting. Serum was obtained after centrifugation of clotted blood samples at 3000 g for 15 min at 4 °C and stored at -80 °C. At the same time-points (7, 14, 21, or 28 days after injection), lungs, liver, and kidneys were harvested, fixed in 10% neutral buffered formalin, paraffin embedded, sectioned and properly stained.

Syngeneic murine neuroblastoma A/J mouse model

A/J female mice (5–6 weeks old) were purchased from Envigo (Bresso, Italy) and maintained at 22–24 °C under pathogen-limiting conditions. Mice were given a standard diet and water *ad libitum* and acclimatized for 2–3 weeks before the start of experiments. Housing and all procedures involving the mice were performed according to the protocol approved by the Institutional Animal Care and Use Committee (Authorization n°385/2023-PR).

For subcutaneous growth, 2×10^6 exponentially growing NXS2 CTRL or hLGALS3BP were s.c. inoculated into the right flank of the mice. Once tumors reached approximately 100 mm³ tumor volume, animals were randomly divided into groups and intravenously injected with vehicle (PBS), naked 1959-sss (10 mg/kg), or ADC 1959-sss/DM4 (10 mg/kg), or intra-peritoneally injected with anti-PD-1 (10 mg/kg). Doses and schedules are described in the individual figure legends. Mice were weighed twice weekly to monitor possible signs of toxicity. Tumor volume was monitored twice weekly by a caliper and

calculated using the following formula: tumor volume (mm³) = (length x width²)/2. A tumor volume of 1-1.5 cm³ was chosen as humane endpoint for all experiments after which mice were sacrificed. Blood was collected just after mice sacrifice to obtain serum and tumors were collected in formalin and embedded in paraffin.

For re-challenge experiments, 2×10^6 exponentially growing NXS2 CTRL cells were s.c. implanted into the left flank of A/J tumor naïve or cured mice. Tumor growth was monitored twice weekly, and tumor volumes were measured using a caliper. A tumor volume of 1-1.5 cm³ was chosen as humane endpoint for all experiments after which mice were sacrificed. Blood was collected just after mice sacrifice to obtain serum and tumors were collected in formalin and embedded in paraffin.

For tumor immunoinfiltrate analysis, A/J female mice were implanted s.c. with 2×10^6 NXS2 hLGALS3BP cells into the right flank. Once tumors reached a volume of approximately 100 mm³, mice were randomly divided into three groups and intravenously treated with vehicle (PBS), naked 1959-sss (10 mg/kg), or ADC 1959-sss/DM4 (10 mg/kg). Two or four mice were treated once or twice, respectively, prior to being sacrificed at 72 h or 7 days from starting treatments and tumors collected for further analysis.

Tumor-infiltrating immune cells (TIIC) analysis in syngeneic neuroblastoma mouse model

For the evaluation of tumor-infiltrating immune cells (TIIC), mice were sacrificed and tumor collected after 72 h or 7 days after the first treatment administration. Tumors were weighed, cut into small pieces and enzymatically dissociated into gentleMACS C tubes (Miltenyi Biotec, Germany) with enzyme mix of mouse Tumor Dissociation Kit (#130-096-730; Miltenyi Biotec) by using a gentleMACS Octo Dissociator with Heaters (#130-096-427; Miltenyi Biotec) using 37C_m_TDK_1 dissociation program. Dissociated tumors were then passed through a 70 µm cell strainer and cell suspensions were centrifuged at 300 g for 7 min; red blood cells were lysed twice for 10 min at RT in agitation with Red Blood Cell lysis solution (#130-094-183; Miltenyi Biotec), then centrifuged at 1200 rpm for 10 min. Cells were counted and approximately 10^7 cells for each sample were incubated with mouse FcR blocking reagent (#130-092-575; Miltenyi Biotec) for 10 min in the refrigerator. Cell suspensions were stained for 30 min at 4 °C with LIVE/DEAD Fixable Near-IR fluorescent dye (#L34975; Invitrogen). For surface antigens staining, cells were incubated for 30 min at 4 °C in BD Brilliant Buffer (#563794; BD Biosciences) with the following antibodies from BD Biosciences: BV711 anti-mouse CD45 (#563709), BV605 anti-mouse CD3e (#563004), BV510 anti-mouse CD4 (#563106), RB705 anti-mouse CD8a (#570255), BV786

anti-CD11b (#569504), PE-CF594 anti-mouse CD49b (#562453), BV421 anti-mouse CD69 (#562920), RB780 anti-mouse CD11c (#755338). After washing, cells were fixed and permeabilized with BD Cytofix/Cytoperm Fixation/Permeabilization kit (#554714; BD Biosciences) according to manufacturer's instructions and then intracellularly labelled with APC anti-Granzyme B REAfinity (Miltenyi Biotec) for 30 min at 4 °C. After washing, cells were finally stained with SYTO16 (#S7578; Molecular Probes, Life Technologies, Thermo-Fisher) for nucleated cells and acquired with a CytoFLEX cytometer (Beckman Coulter, USA). All antibodies and probes were titrated under assay conditions, to obtain optimal dilutions. Concentrations of each antibody used are reported in Supplementary Table S1. Flow cytometer performance, stability, and data reproducibility were checked by using Daily QC Fluorospheres (#C65719, Beckman Coulter, USA). Compensations were calculated using Versa-Comp Antibody Capture Kit (B22804, Beckman Coulter, USA) [23, 24]. Carryover between samples was prevented by appropriate instrument cleaning at the end of each sample acquisition. In order to assess non-specific fluorescence, fluorescence minus one samples (FMO) were used. Samples were analyzed using FlowJo v. 10.10 (BD Biosciences). Boolean gates were used to identify all cell subpopulations. Gating strategy hierarchy and representative gating strategy used are reported in Supplementary Figures S2 and S3.

1959-sss/DM4 conjugation and characterization

1959-sss antibody (MediaPharma Srl, Italy), previously described (US 2008/0305044 A1) [22, 25], was reduced with a 60-fold molar excess of TCEP (Tris(2-carboxyethyl)phosphine; Thermo Fisher Scientific) in phosphate-buffered saline (PBS, pH 7.4; Sigma-Aldrich). The reaction was carried out overnight at RT. To stabilize the reduced antibody and prevent precipitation, 100 mM phosphate buffer (pH 7.4) was added. The reduced antibody was then incubated with a 100-fold molar excess of DTNB (5,5'-Dithiobis(2-nitrobenzoic acid); Sigma-Aldrich) overnight at RT. The reaction was quenched by passing the 1959-sss/DTNB mixture through a G25 Sephadex column pre-equilibrated with PBS containing 5% sucrose and 10% DMA (N, N'-dimethylacetamide; Sigma-Aldrich). The DTNB-modified 1959-sss antibody was subsequently reacted with a 10-fold molar excess of thiol-maytansinoid DM4-SH (MedChemExpress) in the same buffer system overnight at RT. The reaction was terminated by adding a 500-fold molar excess of iodoacetamide (Sigma-Aldrich). Unreacted maytansinoid was removed by passing the mixture through a G25 Sephadex column equilibrated with PBS/5% sucrose/10% DMA at a flow rate of 1 ml/min. The final concentration of the ADCs was determined by UV-VIS spectrophotometry

using an extinction coefficient of $\epsilon_{280} = 1.6 \text{ M}^{-1} \text{ cm}^{-1}$. All ADC products were analyzed by SDS-PAGE and Hydrophobic Interaction Chromatography (HIC). Both the naked 1959-sss antibody and the ADCs were analyzed using a MabPac HIC-Butyl column (Thermo Fisher Scientific) equilibrated in 1.5 M ammonium sulfate, 5% isopropanol, and 50 mM sodium phosphate (pH 7.0). Elution was achieved with a linear gradient from 0 to 100% 50 mM sodium phosphate (pH 7.0) with 20% isopropanol at a flow rate of 1 ml/min. The Drug-Antibody Ratio (DAR) was calculated to be 1,6.

Immunohistochemistry (IHC)

Sections were immunostained with anti-human LGALS3BP antibody (#AF2226, R&D). Microwave pretreatment (10 min) in citrate buffer (pH 6.0) was performed for antigen retrieval. The biotinylated horse anti-goat IgG secondary antibody (BA-9500, Vector Laboratories) and the HRP Detection IHC kit (ab93677, Abcam) were used to detect the antigen. After incubation with the chromogen 3,3-diaminobenzidine DAB (K3468, Dako), slides were counterstained in Hematoxylin (CATHE-MM, Biocare Medical) and scanned with Nanozoomer scanner from Hamamatsu. Images were acquired with NDP.view 2 software.

Statistical analysis

IC_{50} values were calculated by using GraphPad Prism 9.0 software (GraphPad Software, Inc., San Diego, CA, USA). For FACS analysis of ICD markers and PD-L1 levels, p values were determined by unpaired Student's t test and $p < 0.05$ was considered as statistically significant. Statistical differences between experimental groups in the *in vivo* analysis of TILs were determined by unpaired Student's t test and $p < 0.05$ was considered as statistically significant. For Kaplan-Meier survival analysis, a Log-rank (Mantel-Cox) test was used to compare each of the groups. All statistical analysis was performed with GraphPad Prism 9.0 software.

Results

Circulating LGALS3BP correlates with neuroblastoma dissemination in a pseudometastatic model

We recently demonstrated that LGALS3BP is largely expressed and secreted by neuroblastoma cells mainly through the release of cancer-associated extracellular vesicles [26]. We therefore wondered whether the circulating protein could be used as a biomarker of this tumor. To this aim, we employed a pseudometastatic mouse model in which LGALS3BP highly expressing human neuroblastoma SKNAS cells were tail-vein injected into mice. Following the experimental scheme shown in Fig. 1A, we were able to detect circulating LGALS3BP, both as associated to EVs and as free protein in serum

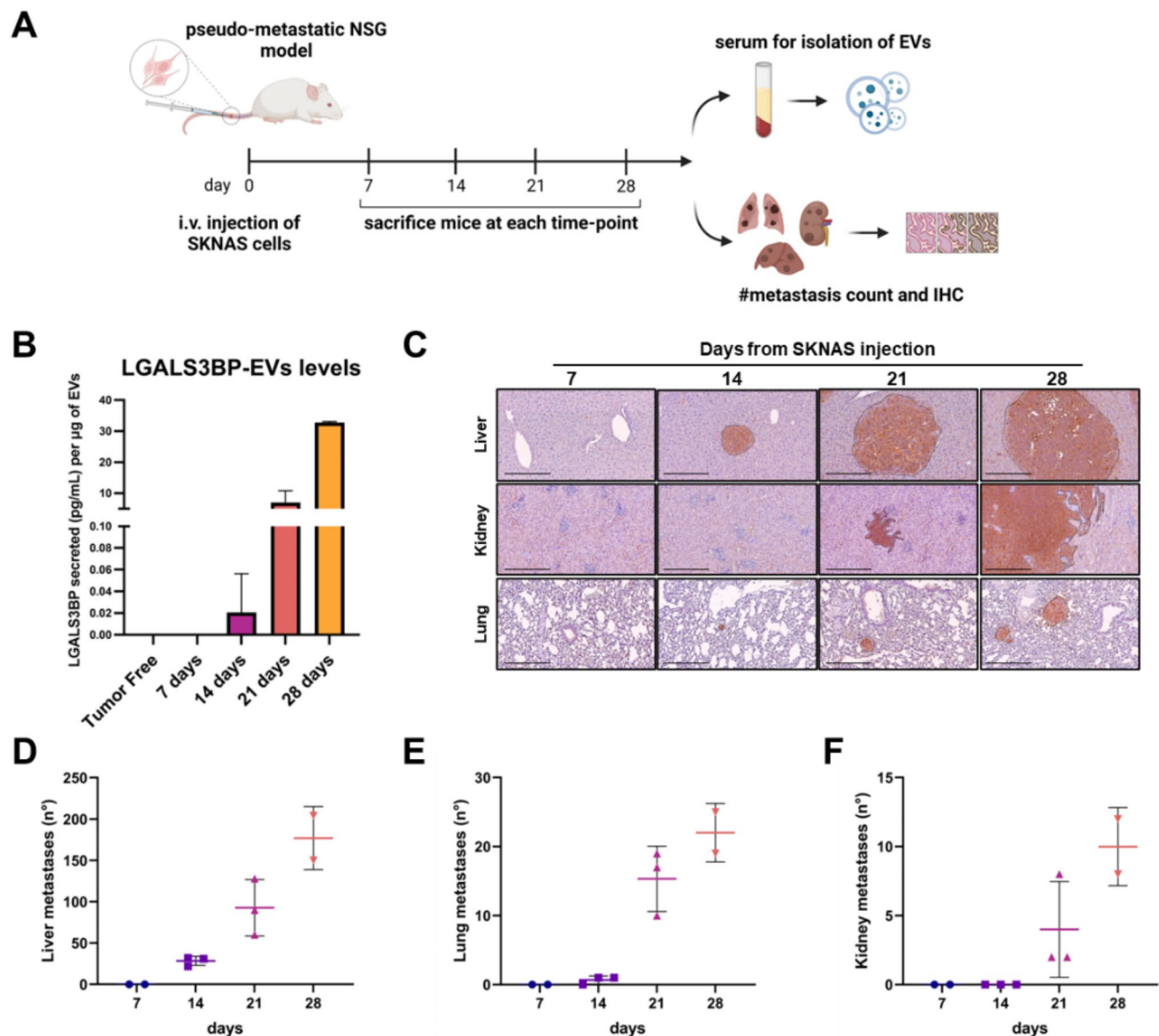


Fig. 1 EVs-associated LGALS3BP levels correlate with metastatic lesions and increase accordingly over time in a pseudometastatic model of human neuroblastoma. **(A)** Representative scheme of pseudometastatic model: human neuroblastoma SKNAS cells were tail-vein injected in NSG mice and blood was collected after 7 ($n=2$), 14 ($n=3$), 21 ($n=3$), and 28 ($n=2$) days. **(B)** EVs-associated LGALS3BP levels detected in ELISA (pg/mL) per µg of EVs isolated from mouse serum after 7 ($n=2$), 14 ($n=3$), 21 ($n=3$), or 28 ($n=2$) days. Tumor free mice ($n=2$) were considered as controls. **(C)** Immunohistochemistry staining with hematoxylin/eosin for metastatic lesions and LGALS3BP levels in metastatic lesions over time. Scale bar: 250 µm. Number of metastases detected in **(D)** liver, **(E)** lung, and **(F)** kidney of NSG mice after 7 ($n=2$), 14 ($n=3$), 21 ($n=3$), and 28 ($n=2$) days

collected from tumor bearing mice (Figs. 1B and Supplementary Figure S1). Interestingly, we found a strong correlation trend over time between circulating LGALS3BP and the number of SKNAS-induced metastatic lesions in liver, lungs and kidneys (Fig. 1C-F). On the contrary, circulating LGALS3BP was undetectable in tumor-free (TF) mice and in SKNAS-injected mice after 7 days (Figs. 1B and Supplementary Figure S1), consistently with the absence of metastatic lesions in the examined organs (Fig. 1C-F).

Next, we evaluated the potential of circulating LGALS3BP as an early detection biomarker for neuroblastoma. We focused on an early time-point, corresponding to 14 days after inoculation of SKNAS cells, in the same pseudometastatic mouse model used before. As shown, we successfully detected EVs-associated LGALS3BP (Figs. 2A-B) and circulating LGALS3BP (Fig. 2C) in serum with high sensitivity given the detection of LGALS3BP levels even in the presence of a minimal number of metastases. In addition, these levels tightly correlated with the number of neuroblastoma

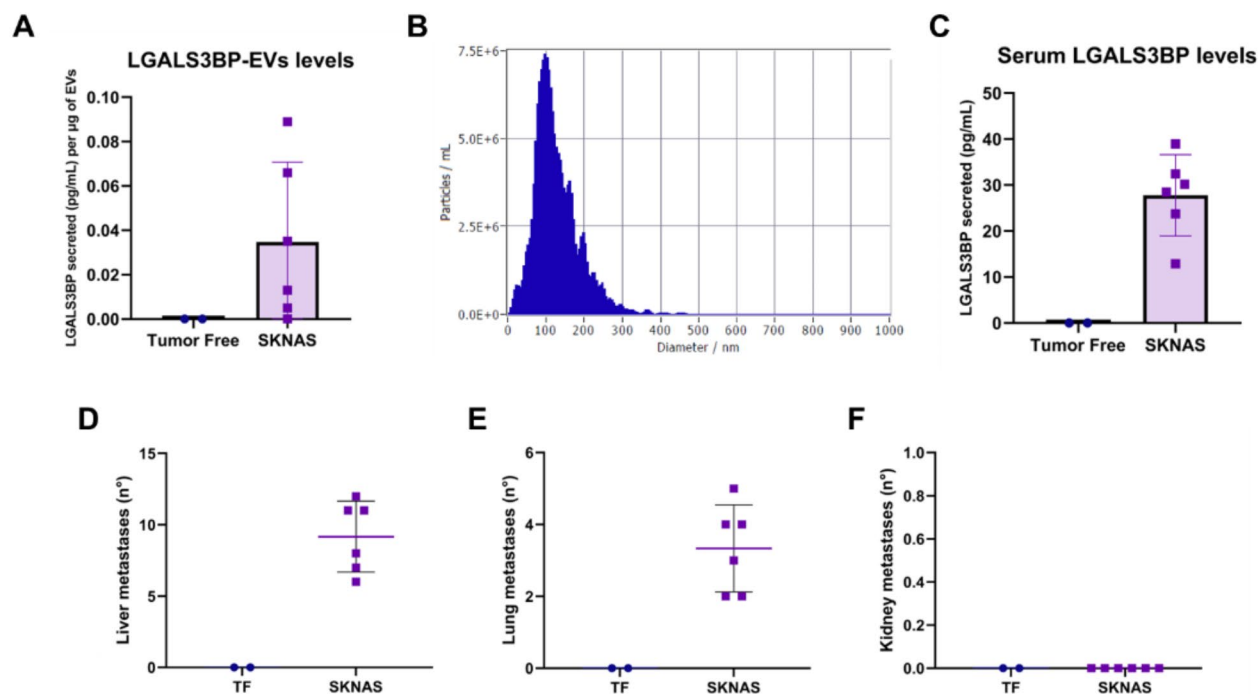


Fig. 2 Circulating and EVs-associated LGALS3BP could function as early detection biomarker of neuroblastoma lesions in a human neuroblastoma pseudometastatic model. **(A)** EVs-associated LGALS3BP levels detected in ELISA (pg/mL) per μg of EVs isolated from mouse serum collected 14 days after NSG mice ($n=6$) were tail-vein injected with human neuroblastoma SKNAS cells. Tumor free mice ($n=2$) were considered as controls. **(B)** Representative NTA profile of EVs isolated from mouse serum after 14 days from tail-vein injection of SKNAS cells. **(C)** Circulating LGALS3BP levels detected in ELISA (pg/mL) in mouse serum (diluted 1:4) after 14 days ($n=6$). Tumor free mice ($n=2$) were considered as controls. Number of metastases detected in **(D)** liver, **(E)** lung, and **(F)** kidney of NSG at 14 days post-injection

lesions observed in mouse organs, with a greater number of metastases identified in the liver and lungs compared to those found in the kidneys (Figs. 2D–F), a result consistent with the higher tropism of SKNAS cells for these organs. As expected, no levels of LGALS3BP were measurable in TF mice. These findings indicate that circulating LGALS3BP levels could serve as a reliable biomarker for neuroblastoma, given the strong correlation observed with the presence of metastases.

Establishment of a murine neuroblastoma cell model with overexpression of human LGALS3BP

The potential of LGALS3BP as a therapeutic target was next investigated. We previously showed that 1959-sss/DM4, an ADC targeting LGALS3BP, was able to halt neuroblastoma growth in several preclinical models [26]. Here, we analyzed the therapeutic activity of this ADC when combined with immunotherapy. First, we generated a syngeneic model by engineering neuroblastoma NXS2 cells through lentiviral transduction. The resulting cell lines were characterized as control (empty vector) or hLGALS3BP. While endogenous expression of murine LGALS3BP was barely detectable in both cell lines, NXS2 hLGALS3BP cells showed a marked overexpression of the protein, as evaluated by mRNA and protein analysis

(Fig. 3A–C). Of note, expression level of the secreted protein was comparable to those of LGALS3BP-high-expressing human cancer cell lines [25–27] (Fig. 3D). At confocal microscopy, the anti-LGALS3BP antibody 1959 intensively and specifically labeled the cell surface/milieu of hLGALS3BP-expressing cells, with no staining in control cells (Fig. 3E). Consistently, EVs isolated from hLGALS3BP-expressing cells showed prominent expression of human LGALS3BP, which was absent in EVs obtained from the control cell line (Fig. 3F).

Cytotoxic payload DM4 induce ICD and PD-L1 expression in murine neuroblastoma cells

To verify NXS2 sensitivity to ravidansine DM4, a cell killing assay was performed. As shown in Fig. 4, this maytansine-derivative cytotoxic compound used as payload for building the anti-LGALS3BP ADC exhibits a potent cytotoxic activity with an IC_{50} in the nanomolar range (0.32 nM), which was the same in both control and hLGALS3BP-expressing cells (Fig. 4A left panel). In contrast, no cytotoxicity was observed in cells treated with the naked 1959 antibody (1959-sss) (Fig. 4A right panel).

The ability of DM4 to induce ICD was evaluated using a sub-lethal drug concentration chosen from the previous IC_{50} curves. For these experiments, NXS2 cells were

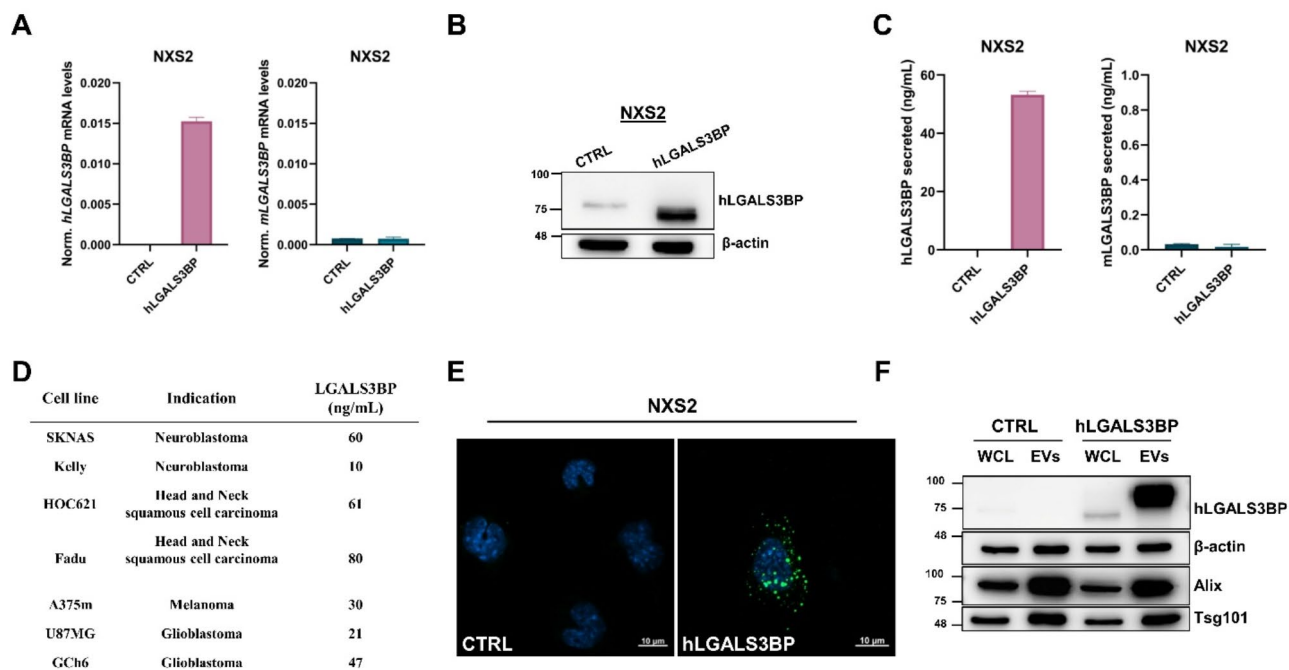


Fig. 3 Human LGALS3BP is overexpressed and secreted by engineered murine neuroblastoma NXS2 hLGALS3BP cells. **(A)** Histograms showing transcriptional levels of human (hLGALS3BP) and murine (mLGALS3BP) LGALS3BP in NXS2 CTRL and hLGALS3BP cells normalized to housekeeping gene (β -actin). Values refer to two independent biological replicates. **(B)** Western blotting images showing intracellular protein levels of hLGALS3BP in NXS2 CTRL and hLGALS3BP cells. Equal amounts of protein were loaded for each sample. β -actin was used as loading control. Images are representative of two independent biological replicates. **(C)** Secreted levels (ng/mL) of hLGALS3BP and mLGALS3BP assessed by ELISA assay in NXS2 CTRL and hLGALS3BP cells. Values refer to two independent biological replicates. **(D)** Table showing secreted LGALS3BP expression level in a panel of human cancer cell lines. **(E)** Confocal imaging of NXS2 CTRL and hLGALS3BP cells showing LGALS3BP (green) and nuclei (Hoechst). Scale bar: 10 μ m. **(F)** Immunoblot showing EV-associated hLGALS3BP and positive/negative exosomal markers expression in whole cell lysates (WCL) or EVs isolated from NXS2 CTRL or hLGALS3BP. Equal amount of protein were loaded for each sample.

exposed to 5nM DM4 for 72 h or to 60 μ M oxaliplatin (OXA) as the ICD-inducer for 48 h, and the expression levels of calreticulin, HSP70, and HSP90 analyzed by flow cytometry. Interestingly, all three ICD markers were significantly upregulated, indicating that DM4 induces ICD in this neuroblastoma cell model (Fig. 4B–D). To gain insight into the potential mechanism of resistance of neuroblastoma cells through the modulation of immune check-point proteins, we analyzed expression of PD-L1 in NXS2 control and hLGALS3BP cells in response to treatment with DM4. A significant upregulation of PD-L1 surface expression in both cell lines was observed, confirming the ability of DM4 to induce a potential resistance mechanism (Fig. 4E).

Anti-LGALS3BP ADC induces shrinkage of neuroblastoma tumors and the recruitment of activated TILs

Next, we wondered whether the antitumor activity of LGALS3BP ADC was maintained in the syngeneic model and, more importantly, whether it was specific for cells expressing the target. We set the ADC dosage at 10 mg/kg twice weekly as the most effective anti-tumor dosage based on our previous works [5, 25, 26, 28]. ADC treatment resulted in a significant shrinkage

of hLGALS3BP-expressing tumors, which was accompanied by an increased survival, but not of control-derived tumors (Fig. 5A and B). However, this effect was not sustained over time, as tumor regrowth was observed two weeks following the final treatment (see Supplementary Materials, sheet “Tumor growth therapeutic”). To determine whether the therapeutic response could be improved by combining the ADC with immunotherapy, we first analyzed the composition of the tumor infiltrate in animals treated with two doses of the ADC after 7 days from starting of treatments. The analysis was conducted within the time window corresponding to the maximum response to the drug. As shown in Fig. 5C, NXS2-hLGALS3BP tumors treated with anti-LGALS3BP ADC displayed a significant increase in activated tumor-infiltrating T lymphocytes (TILs), as evidenced by flow cytometry analysis of CD69⁺/CD45⁺CD3⁺ cells. Furthermore, ADC-treated tumors showed a marked enhancement in the CD8⁺/CD69⁺ and CD8⁺/CD69⁺/Granzyme B⁺ cell subpopulation frequencies, which represents the primary T-cell population involved in the anti-tumor immune response. Gating strategy for the analysis of tumor infiltrate is shown in Supplementary Figure S3.

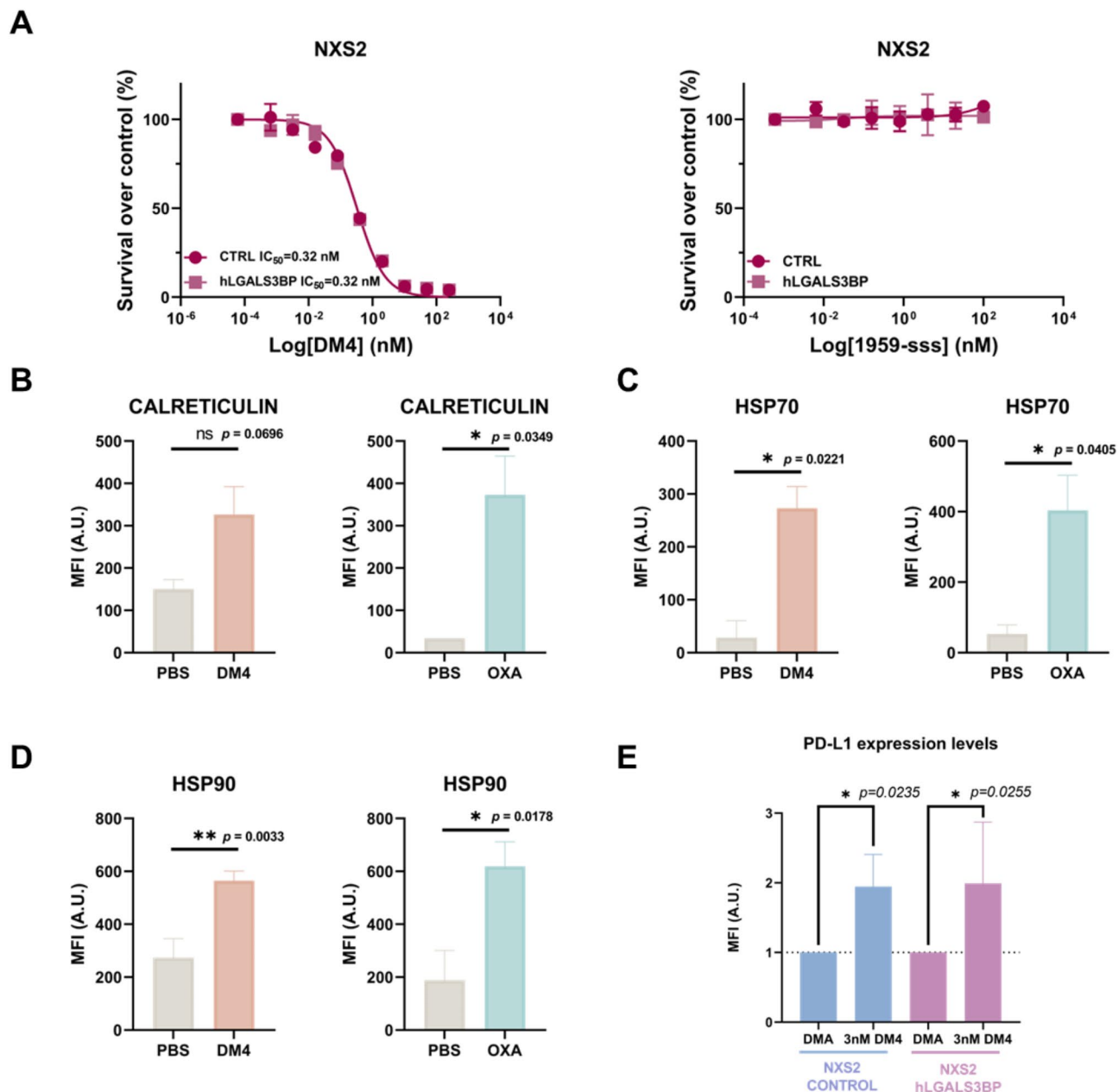


Fig. 4 NXS2 cells are susceptible to the cytotoxic payload DM4 and expose immunogenic cell death (ICD) markers after treatment with DM4, which may also induce tumor resistance in NXS2 cell lines by upregulation of PD-L1. **(A)** In vitro IC_{50} curves assessed through cytotoxicity assays by exposing for 72 h NXS2 CTRL and hLGALS3BP cells to increasing doses of payload DM4 (left panel) or naked 1959-sss antibody (right panel). IC_{50} values are reported for each cell line considered upon the different treatments. Values refer to two independent biological replicates. Surface levels of ICD markers **(B)** calreticulin, **(C)** HSP70, and **(D)** HSP90 expressed as mean fluorescence intensity (M.F.I.) signals evaluated through FACS analysis on NXS2 cells treated or not with DM4 5nM for 72 h or with Oxaliplatin (OXA) 60 μ M for 48 h. Asterisks indicate statistical significance through unpaired t-test compared to each experimental time control (PBS); * $p < 0.05$, ** $p < 0.01$. Exact p -values are reported. Values refer to two or three independent biological replicates. **(E)** Surface levels of PD-L1 evaluated through FACS analysis expressed as fold change of mean fluorescence intensity (M.F.I.) signals of treated samples over controls of NXS2 control and hLGALS3BP cells treated with 3nM DM4 or with DMA (control) for 72 h. Asterisks indicate statistical significance through unpaired t-test compared to each experimental control (DMA); * $p < 0.05$. Exact p -values are reported. Values refer to three independent biological replicates

Anti-LGALS3BP synergizes with anti-PD-1 immunotherapy promoting durable anti-tumor activity

These findings provided a rationale for evaluating the effect of combination therapy of the ADC with an immune check-point inhibitor. In this respect, we

decided to test 1959-sss/DM4 in combination with immune check-point inhibitor anti-PD-1, with a six-arm therapeutic trial comparing the effects of monotherapy with those of the combination of ADC and anti-PD-1 on NXS2-hLGALS3BP-derived tumors. We used the same

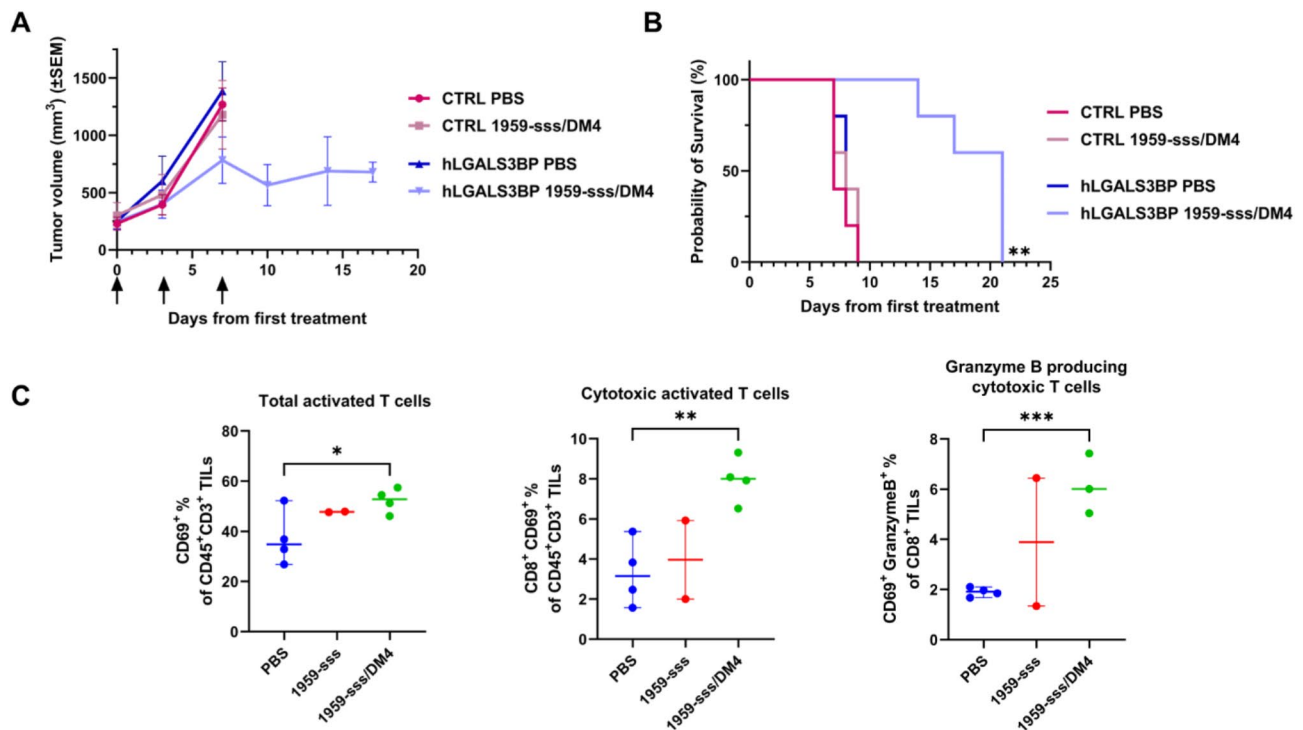


Fig. 5 Targeted and effective anti-tumor activity of anti-LGALS3BP ADC 1959-sss/DM4 in murine syngeneic neuroblastoma model. **(A)** Tumor growth expressed as tumor volume (mm³) from first treatment of NXS2 CTRL or hLGALS3BP allografts in syngeneic A/J mice treated or not with ADC 1959-sss/DM4 (10 mg/kg; twice weekly; three total i.v. injections). Arrows indicate treatments administration. 4 or 5 mice per group were considered. **(B)** Kaplan-Meier curve showing probability of survival in percentage of mice bearing NXS2 CTRL or hLGALS3BP allografts treated or not with ADC 1959-sss/DM4 from first treatment. Log-rank (Mantel-Cox) test: ** $p < 0.01$. **(C)** TILs flow cytometric analysis of PBS ($n = 4$), 1959-sss ($n = 2$) and 1959-sss/DM4 ($n = 4$) treated tumors at 7 days after starting treatments, showing percentage of activated CD69⁺ within the total population of CD3⁺T cells (left panel); percentage of activated CD8⁺CD69⁺ within the total population of CD3⁺T cells (middle panel). In the right panel is shown the percentage of CD69⁺ Granzyme B⁺ over cytotoxic CD8⁺T cells. Differences were compared using unpaired T test, and considering significant $p < 0.05$, as indicated with an asterisk (* $p < 0.05$, ** $p < 0.01$, *** $p < 0.001$)

ADC dosage of the previous therapeutic experiment (10 mg/kg, twice weekly) while we built anti-PD-1 treatments schedule by setting dosage at 10 mg/kg with two injections per week based on other prior combination immunotherapy works [29–31]. A significant enhancement of antitumor activity was observed in mice treated with the combination therapy compared to those treated with the single agents, which resulted in prolonged survival up to 60 days from the start of treatment (Fig. 6A–B). Of note, in the combo group, 4 out of 6 mice were cured after 60 days from the start of the treatment.

To verify whether these cured mice still possessed immune memory against the tumor, we used them as rechallenge models (Fig. 7). We injected parental NXS2 cells in the 4 cured mice and as control in two “naïve” animals. Tumors in the cured mice exhibited slower growth and reduced attachment efficiency compared to those in naïve mice, as evidenced by smaller tumor volumes 14 days post-injection and the failure of one tumor in the cured group to attach and grow. All these observations strongly suggest that the cured mice may possess a stronger or more efficient immune response that contributed

to controlling tumor growth (Fig. 7B). Moreover, a significant response, marked by initial tumor shrinkage, was observed in mice bearing tumors when treated with anti-PD-1 therapy (administered in three doses) (Fig. 7), indicating that these mice had a heightened or ‘primed’ immune state due to the earlier treatment, which made them more responsive to the immune check-point blockade therapy compared to naïve mice treated in the previous experiment (Fig. 6A).

Discussion

Neuroblastoma is often driven by specific genetic mutations and remains extremely challenging to treat [32]. Children with this aggressive form of the disease typically undergo intensive therapies, which are not always successful [33]. Tragically, nearly half of these patients do not survive beyond the age of five. For survivors, the lifesaving but harsh treatments frequently result in permanent side effects, significantly impacting their quality of life [34]. These challenges underscore the urgent need for more effective therapies and the development of novel

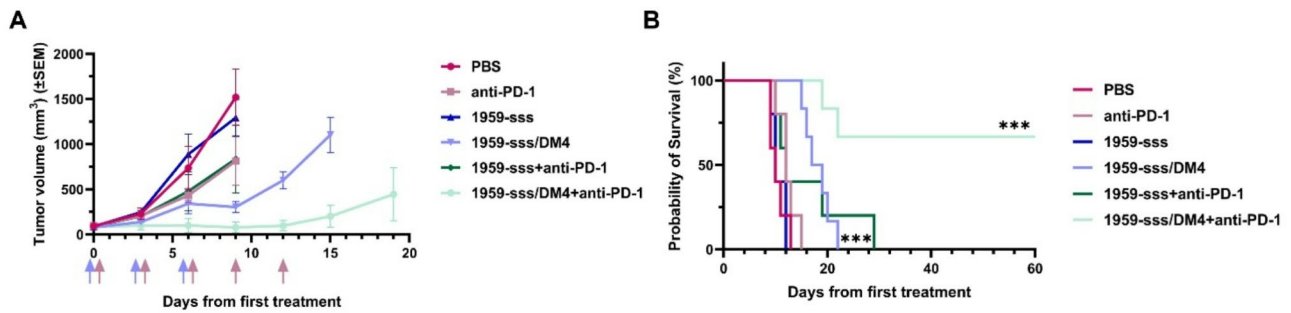


Fig. 6 Synergistic and durable anti-tumor activity of combination therapy based on anti-LGALS3BP ADC 1959-sss/DM4 and immune check-point inhibitor anti-PD-1 in murine syngeneic neuroblastoma model. **(A)** Tumor growth expressed as tumor volume (mm^3) from first treatment of NX52 hLGALS3BP allografts in syngeneic A/J mice treated or not with anti-PD-1 (10 mg/kg; twice weekly; five total i.p. injections), naked 1959-sss (10 mg/kg; twice weekly; three total i.v. injections), ADC 1959-sss/DM4 (10 mg/kg; twice weekly; three total i.v. injections), or combination of 1959-sss and anti-PD-1, or combination of 1959-sss/DM4 and anti-PD-1. Blue and pink arrows indicate 1959-sss or 1959-sss/DM4 and anti-PD-1 treatments administration, respectively. 5 or 6 mice were considered per experimental group. **(B)** Kaplan-Meier curve showing probability of survival of mice bearing NX52 hLGALS3BP allografts treated or not with anti-PD-1, 1959-sss, ADC 1959-sss/DM4, combination of 1959-sss and anti-PD-1, or combination of 1959-sss/DM4 and anti-PD-1 from first treatment. Log-rank (Mantel-Cox) test: *** $p < 0.001$

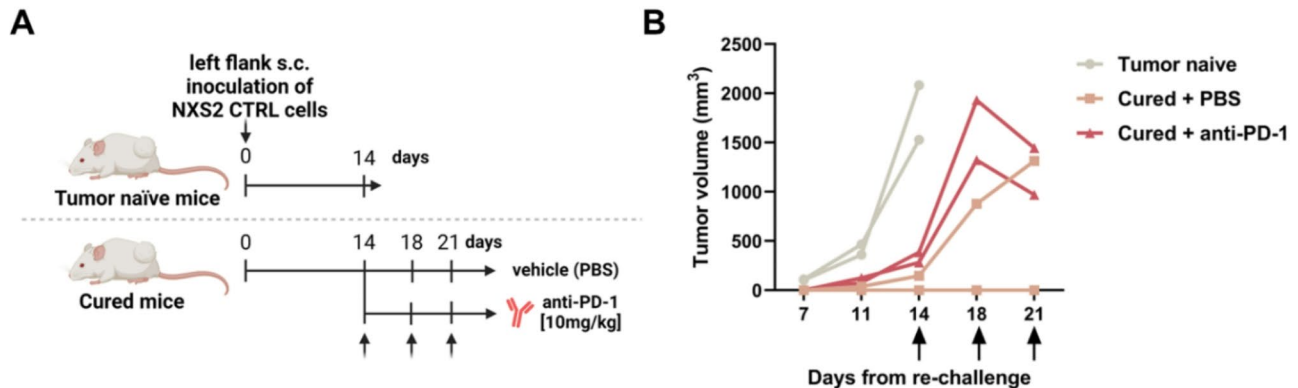


Fig. 7 Cured mice displayed superior tumor growth control compared to naïve animals. **(A)** Representative scheme of rechallenge experiment. Cured mice are those animals that show complete tumor regression from combination therapy with 1959-sss/DM4 + anti-PD-1. **(B)** Tumor growth expressed as tumor volume (mm^3) from rechallenge of NX52 CTRL allografts in tumor naïve mice, cured mice treated with PBS, or cured mice treated with anti-PD-1. Arrows indicate administration of vehicle (PBS) or anti-PD-1 (10 mg/kg; twice weekly; three total i.p. injections). Two mice were considered per experimental group and curves reported refer to tumor growth of allografts of each single animal considered per group

targeted approaches, combined with reliable biomarkers for disease monitoring.

In this study, we investigated the potential of LGALS3BP protein as a disease biomarker. Our results demonstrate that circulating LGALS3BP can serve as an effective liquid biopsy biomarker for detecting the presence of the disease. Additionally, we show that an ADC-based therapy displays a synergistic effect when combined with an immune check-point inhibitor, holding promising clinical relevance for neuroblastoma treatment.

Our group, along with others, has identified LGALS3BP as a driver of tumor progression in various cancers, including neuroblastoma, due to its role in sustaining cancer proliferation, modulating cell motility and adhesion within the tumor microenvironment, and promoting angiogenesis (reviewed by Capone et al. [16]). Previous studies investigating protein downregulation have

demonstrated that these mechanisms are significantly reduced or impaired, further reinforcing the notion that LGALS3BP plays an active role in tumor progression [35–39]. Importantly, LGALS3BP was found as a critical mediator in the interaction between neuroblastoma cells and the TME [18, 19]. LGALS3BP is a predominant surface component of cancer-derived EVs. These EVs play a significant role in shaping a particular type of TME that promotes cancer progression to which they also contribute by facilitating immune escape, stimulating angiogenesis, and preparing the pre-metastatic niche [40]. This evidence underscores LGALS3BP's involvement in neuroblastoma pathophysiology, making it a compelling target for therapeutic intervention and a valuable biomarker for monitoring disease dynamics.

Using a neuroblastoma pseudometastatic preclinical model, we demonstrate that EVs-associated LGALS3BP correlates with disease progression and dissemination.

These findings align with a recent study by Morini and colleagues, which reported upregulation of LGALS3BP in extracellular vesicles isolated from high-risk neuroblastoma patients compared to controls [41]. Moreover, we found that 1959-sss/DM4 LGALS3BP ADC possesses immune-modulating properties, by showing that ravidanin DM4 is able to induce ICD. Our findings clearly highlight the potential of ADC/immune check-point combination strategy in neuroblastoma. Recently, Pasto et al. showed that pyrrolbenzodiazepine (PBD)-based GD2 ADC induces ICD mainly by reprogramming tumor milieu. In our setting, a DM4-armed anti-LGALS3BP ADC is directed against a vesicular highly glycosylated protein which is enriched at the tumor surface and in stroma. 1959-sss/DM4 is a linker-less ADC with a fixed DAR around 2, which has demonstrated potent antitumor activity against different malignancies, including melanoma, neuroblastoma, glioblastoma and adenoid cystic carcinoma [5, 25, 26, 28]. Importantly, this ADC has demonstrated potent, target-dependent antitumor activity and high tolerability in multiple mouse pre-clinical models [5, 25, 26, 28]. Furthermore, previous exploratory toxicology studies in rabbits, where the 1959 antibody cross-reacted with endogenous LGALS3BP protein, reported no mortality or treatment-related toxicity [25].

To highlight the ADC's ability to modify the immune landscape of treated tumors, we employed the A/J syngeneic model. As a cellular model, we engineered murine neuroblastoma NXS2 cells to overexpress the human LGALS3BP protein. This step was essential to establish a reliable preclinical model because: (i) murine neuroblastoma cells inherently express very low levels of the ADC target, and (ii) the 1959 monoclonal antibody does not cross-react with murine LGALS3BP.

One of the aims of the present study was to evaluate whether DM4 payload possesses the capacity to induce ICD in the context of neuroblastoma. To date, there is only one study addressing this specific matter [42]. ICD is a widely investigated mechanism in ADC therapy, as strong immune modulation induced by the payload provides a compelling rationale for combining ADCs with ICIs. In our syngeneic model, ADC treatment resulted in a substantial increase in tumor-infiltrating lymphocytes (TILs) within the tumor tissue. Notably, treatment with the anti-LGALS3BP ADC resulted in a significant enrichment of activated cytotoxic T-lymphocytes (CD69⁺/GranzymeB⁺ subpopulation) in tumor tissue, strongly supporting the potential for enhancing ADC activity through immunotherapy.

Indeed, the combination of the ADC with anti-PD-1 resulted in a significant boost of antitumor activity with prolonged survival of treated mice. Four out of six mice treated with the combination therapy remained

tumor-free 60 days after the start of treatment, whereas animals in the control group reached the tumor growth cut-off value by day 15. Using a rechallenge model, we tested whether cured mice had developed immune memory against the tumor. Importantly, we observed two key phenomena: (i) tumor growth was significantly delayed in 'cured' mice compared to naïve animals, indicating the presence of immune memory; and (ii) tumors in these mice exhibited increased sensitivity to anti-PD-1 monotherapy, suggesting an enhanced antitumor immune response. This suggests that these mice had a heightened or 'primed' immune state due to the earlier treatment, which made them more responsive to the immune check-point blockade therapy compared to naïve mice (as shown in Fig. 6A). This implies that immune memory induced by the ADC facilitated a more effective immune response upon reactivation with anti-PD-1 therapy. This reinforces the idea that initial treatment with the ADC, which is followed by ICD induction, can prime the immune system and enhances the efficacy of subsequent immunotherapy. However, the intrinsic limitations of these experimental settings must be considered, as we are forcing a system in which a human protein interacts with a murine TME, which may not fully reflect the dynamics of a patient's TME. Nevertheless, this is a common limitation of all preclinical models used to evaluate the impact of immunotherapies on TME immune cells.

Although these preclinical findings are encouraging, many challenging issues need to be addressed for ADC clinical translation. One potential issue is the emergence of ADC resistance, which can arise through various mechanisms, including antigen-related resistance, disruptions in ADC trafficking pathways, overexpression of drug transporter proteins, and other adaptive processes. To date, there are two FDA-approved antibody-maytansinoid conjugates (AMCs) and several others on preclinical development [43]. However, such in the case of trastuzumab emtansine (T-DM1), dysfunctional intracellular processing of T-DM1 or altered DM1-induced cell death due to higher drug efflux or mutations in DM1 molecular targets were all reported as maytansinoid-related resistance mechanisms [44]. Similarly, DM4-armed ADC resistance could arise for the same reasons. In this context, combination therapies might improve the design of therapeutic strategies to limit resistance issues. As a supporting tool, the discovery of biomarkers able to monitor the therapeutic response and the possible onset of resistance mechanisms could be useful. In relation to this, an intriguing aspect of anti-LGALS3BP therapy with ADCs is the potential use of circulating protein levels as a biomarker to monitor therapeutic response. Furthermore, we recently demonstrated that this ADC, labeled with Zirconium-89, effectively visualized LGALS3BP-secreting tumors in preclinical models using PET

imaging. Therefore, it has the potential to serve as a companion theranostic for identifying patients most likely to respond to LGALS3BP-targeted therapeutics, such as 1959-sss/DM4 [45].

In sum, this study highlights two aspects of LGALS3BP which have an important role in neuroblastoma: (i) the ability to act as a circulating biomarker and (ii) the potential to serve as a therapeutic target in strategies combining ADC therapy with immunotherapy. Both these aspects warrant further exploration.

Supplementary Information

The online version contains supplementary material available at <https://doi.org/10.1186/s12967-025-06434-1>.

Supplementary Material 1

Supplementary Material 2

Acknowledgements

We thank Cosmo Rossi, Francesco Del Pizzo, Valentina Pasi, for their assistance in animal studies and immunohistochemistry assays. We are indebted to Prof. Alessandro Cama and Dr. Serena Veschi for their support in characterizing extracellular vesicles through nanoparticle tracking analysis.

Author contributions

IC: performed the experiments, interpreted data, wrote the manuscript; EC: investigation, data curation; AP: investigation, data curation; GL: performed purification of the antibody, conjugation and analytic characterization of the ADC; PS: performed cytofluorimetry experiments; MC: performed purification of the antibody, conjugation and analytic characterization of the ADC; AL: investigation, data curation; AP: performed NTA; MI: data interpretation, critical revision; PL: data interpretation, critical revision; VdL: funding acquisition, critical revision; RI: data curation; critical revision; SI: suggested ideas and wrote the paper; GS: designed the study, supervised the project and wrote the paper.

Funding

This work was supported by Fondazione-AIRC: GS [IG 2021 id 25696].

Data availability

All data generated or analyzed during this study are included in this published article.

Declarations

Conflict of interest

GS and SI are shareholders of Mediapharma s.r.l. and the other authors declare that they have no conflict of interest in this study.

Author details

¹Department of Innovative Technologies in Medicine & Dentistry, "G. d'Annunzio" University of Chieti-Pescara, Chieti, Italy

²Center for Advanced Studies and Technology (CAST), "G. d'Annunzio" University of Chieti-Pescara, Chieti, Italy

³Department of Science, "G. d'Annunzio" University of Chieti-Pescara, Via Luigi Polacchi, 11, Chieti Scalo, Chieti 66100, Italy

⁴Department of Medicine and Aging Sciences, G. d'Annunzio University of Chieti-Pescara, 66100 Chieti, Italy

⁵Department of Life, Health and Environmental Sciences, University of L'Aquila, 67100 Coppito, Italy

⁶Department of Neurosciences, Imaging and Clinical Sciences, "G. d'Annunzio" University of Chieti-Pescara, Via Luigi Polacchi, 11, Chieti Scalo, Chieti 66100, Italy

⁷Department of Pharmacy, "G. d'Annunzio" University of Chieti-Pescara, 66100 Chieti, Italy

⁸MediaPharma s.r.l, Via Colonna 50/A, Chieti, Italy

Received: 13 January 2025 / Accepted: 26 March 2025

Published online: 11 April 2025

References

1. Pieniżek B, et al. Neuroblastoma—A review of combination immunotherapy. *Int J Mol Sci.* 2024;25(14):7730.
2. DuBois SG, Macy ME, Henderson TO. High-Risk and relapsed neuroblastoma: toward more cures and better outcomes. *Am Soc Clin Oncol Educ Book.* 2022;42:1–13.
3. Weiser DA, et al. Progress toward liquid biopsies in pediatric solid tumors. *Cancer Metastasis Rev.* 2019;38(4):553–71.
4. Trigg RM, Shaw JA, Turner SD. Opportunities and challenges of Circulating biomarkers in neuroblastoma. *Open Biol.* 2019;9(5):190056.
5. Dufresine B et al. Extracellular LGALS3BP: a potential disease marker and actionable target for antibody-drug conjugate therapy in glioblastoma. *Mol Oncol.* 2023.
6. Zhuo Z, et al. Advances in liquid biopsy in neuroblastoma. *Fundam Res.* 2022;2(6):903–17.
7. Kalluri R, LeBleu VS. The biology, function, and biomedical applications of exosomes. *Science.* 2020. 367(6478).
8. Krystal J, Foster JH. Treatment of High-Risk neuroblastoma. *Children.* 2023;10(8):1302.
9. Davis KL, et al. Nivolumab in children and young adults with relapsed or refractory solid tumours or lymphoma (ADVL1412): a multicentre, open-label, single-arm, phase 1–2 trial. *Lancet Oncol.* 2020;21(4):541–50.
10. Grobner SN, et al. The landscape of genomic alterations across childhood cancers. *Nature.* 2018;555(7696):321–7.
11. Apps JR, et al. The immune environment of paediatric solid malignancies: evidence from an immunohistochemical study of clinical cases. *Fetal Pediatr Pathol.* 2013;32(4):298–307.
12. Wienke J, et al. The immune landscape of neuroblastoma: challenges and opportunities for novel therapeutic strategies in pediatric oncology. *Eur J Cancer.* 2021;144:123–50.
13. Pascual-Pasto G, et al. GPC2 antibody–drug conjugate reprograms the neuroblastoma immune milieu to enhance macrophage-driven therapies. *J Immunother Cancer.* 2022;10(12):e004704.
14. Zhang L, et al. Antibody–drug conjugates and immune checkpoint inhibitors in cancer treatment: a systematic review and meta-analysis. *Sci Rep.* 2024;14(1):22357.
15. Galluzzi L, et al. Immunogenic cell death in cancer: concept and therapeutic implications. *J Translational Med.* 2023;21(1):162.
16. Capone E, Iacobelli S, Sala G. Role of galectin 3 binding protein in cancer progression: a potential novel therapeutic target. *J Transl Med.* 2021;19(1):405.
17. Nakata R, et al. Contribution of neuroblastoma-derived exosomes to the production of pro-tumorigenic signals by bone marrow mesenchymal stromal cells. *J Extracell Vesicles.* 2017;6(1):1332941.
18. Silverman AM, et al. A galectin-3-dependent pathway upregulates interleukin-6 in the microenvironment of human neuroblastoma. *Cancer Res.* 2012;72(9):2228–38.
19. Fukaya Y, et al. Identification of galectin-3-binding protein as a factor secreted by tumor cells that stimulates interleukin-6 expression in the bone marrow stroma. *J Biol Chem.* 2008;283(27):18573–81.
20. Greene LA, et al. Neuronal properties of hybrid neuroblastoma X sympathetic ganglion cells. *Proc Natl Acad Sci U S A.* 1975;72(12):4923–7.
21. Campeau E, et al. A versatile viral system for expression and depletion of proteins in mammalian cells. *PLoS ONE.* 2009;4(8):e6529.
22. Traini S, et al. Inhibition of tumor growth and angiogenesis by SP-2, an anti-galectin, galactoside-binding soluble 3 binding protein (LGALS3BP) antibody. *Mol Cancer Ther.* 2014;13(4):916–25.
23. Lanuti P et al. Picture of the favourable immune profile induced by Anti-SARS-CoV-2 vaccination. *Biomedicines.* 2021. 9(8).
24. Lanuti P, et al. A standardized flow cytometry network study for the assessment of Circulating endothelial cell physiological ranges. *Sci Rep.* 2018;8(1):5823.
25. Giansanti F, et al. Secreted Gal-3BP is a novel promising target for non-internalizing Antibody-Drug conjugates. *J Control Release.* 2019;294:176–84.

26. Capone E et al. Targeting vesicular LGALS3BP by an Antibody-Drug conjugate as novel therapeutic strategy for neuroblastoma. *Cancers (Basel)*, 2020. 12(10).
27. Cela I, et al. LGALS3BP is a potential target of antibody-drug conjugates in oral squamous cell carcinoma. *Oral Dis.* 2024;30(4):2039–50.
28. Capone E, et al. Anti-LGALS3BP antibody-drug conjugate treatment induces durable and potent antitumor response in a preclinical model of adenoid cystic carcinoma. *Oral Oncol.* 2024;148:106635.
29. Rigo V, et al. Combined immunotherapy with anti-PDL-1/PD-1 and anti-CD4 antibodies cures syngeneic disseminated neuroblastoma. *Sci Rep.* 2017;7(1):14049.
30. Ivasko SM et al. Combination of GD2-directed bispecific trifunctional antibody therapy with Pd-1 immune checkpoint Blockade induces anti-neuroblastoma immunity in a syngeneic mouse model. *Front Immunol.* 2023. 13.
31. Haratani K, et al. U3-1402 sensitizes HER3-expressing tumors to PD-1 Blockade by immune activation. *J Clin Investig.* 2020;130(1):374–88.
32. Krystal J, Foster JH. Treatment of High-Risk neuroblastoma. *Child (Basel)*, 2023. 10(8).
33. Qiu B, Matthey KK. Advancing therapy for neuroblastoma. *Nat Rev Clin Oncol.* 2022;19(8):515–33.
34. Wahba A, Wolters R, Foster JH. Neuroblastoma in the era of precision medicine: A clinical review. *Cancers (Basel)*, 2023. 15(19).
35. Liu Y, et al. Aberrant expression of LGALS3BP drives an unfavorable prognosis and more aggressive in HCC via regulating PI3K/AKT signaling. *Tissue Cell.* 2024;89:102471.
36. Li L, et al. LGALS3BP is a novel and potential biomarker in clear cell renal cell carcinoma. *Aging.* 2024;16(4):4033–51.
37. Choi Y-S et al. Antibody-mediated blockade for galectin-3 binding protein in tumor secretome abrogates PDAC metastasis. *Proceedings of the National Academy of Sciences.* 2022;119(30):e2119048119.
38. Kim S-S, et al. Secreted LGALS3BP facilitates distant metastasis of breast cancer. *Breast Cancer Res.* 2025;27(1):4.
39. Piccolo E, et al. LGALS3BP, lectin galactoside-binding soluble 3 binding protein, induces vascular endothelial growth factor in human breast cancer cells and promotes angiogenesis. *J Mol Med (Berl).* 2013;91(1):83–94.
40. Kalluri R, McAndrews KM. The role of extracellular vesicles in cancer. *Cell.* 2023;186(8):1610–26.
41. Morini M, et al. Plasma-Derived exosome proteins as novel diagnostic and prognostic biomarkers in neuroblastoma patients. *Cells.* 2023;12(21):2516.
42. Nicolazzi C, et al. Abstract 3740: Tusamitamab Ravtansine induces Immunogenic cell death and synergizes with anti-PD-1 or anti-PD-L1 antibody combination in solid tumor. *Cancer Res.* 2024;84(6Supplement):3740–3740.
43. Perra M, et al. Maytansinoids in cancer therapy: advancements in antibody-drug conjugates and nanotechnology-enhanced drug delivery systems. *Discov Oncol.* 2025;16(1):73.
44. García-Alonso S, Ocaña A, Pandiella A. Trastuzumab Emtansine: mechanisms of action and resistance, clinical progress, and beyond. *Trends Cancer.* 2020;6(2):130–46.
45. Keinänen O, et al. Visualizing Galectin-3 binding protein expression with ImmunoPET. *Mol Pharm.* 2023;20(6):3241–8.

Publisher's note

Springer Nature remains neutral with regard to jurisdictional claims in published maps and institutional affiliations.